NRC Research Press

ARTICLE

Provenance and depositional environment of organic-rich calcareous black shale of the Late Ordovician Macasty Formation, western Anticosti Basin, eastern Canada[1]

Keiko Hattori, André Desrochers, and Janice Pedro

Abstract: The organic-rich Macasty shale in the Gulf of St. Lawrence was deposited in the Late Ordovician during the Taconic orogeny. The orogeny involved explosive volcanism and thrusting of allochthonous rocks in the eastern margin of North America. Neodymium isotope compositions of the shale show that the provenance is predominantly Grenvillian granite–gneissic rocks, which were widely exposed north of the basin, with little contribution from Taconic igneous rocks. The bulk composition and the presence of detrital kaolinite suggest that the Grenvillian source rocks underwent intense weathering before erosion. Fine-grained detritus was deposited in the Anticosti Basin, where abundant organic activity kept the sediment–water interface under anoxic conditions. This proposed interpretation is supported by the enrichment of redox-sensitive elements, such as As, V, and U, and by high $\delta^{34}S$ for pyrite. Calcite cement formed in the pore space of sediments during the diagenesis at temperatures below 60 °C. The low-temperature diagenetic conditions are consistent with the preservation of abundant organic matter in the shale.

Résumé : Le shale riche en matière organique de Macasty dans le golfe du Saint-Laurent a été déposé à l'Ordovicien tardif durant l'orogenèse taconique, qui est caractérisée par un volcanisme explosif et le chevauchement de roches allochtones à la bordure est de l'Amérique du Nord. La composition des isotopes du néodyme dans le shale montre qu'il provient principalement de roches granitiques-gneissiques grenvilliennes qui étaient exposées à grande échelle au nord du bassin, sans grande contribution de roches ignées taconiques. La composition globale et la présence de kaolinite détritique donnent à penser que les roches sources grenvilliennes ont subi une altération météorique intense avant d'être érodées. Les détritus fins ont été déposés dans le bassin d'Anticosti, où l'abondante activité organique a maintenu l'interface sédiments-eau dans des conditions anoxiques. L'interprétation proposée est appuyée par l'enrichissement d'éléments sensibles aux conditions d'oxydoréduction, comme l'As, le V, l'U, ainsi que par le $\delta^{34}S$ élevé de la pyrite. Du ciment de calcite s'est formé dans l'espace interstitiel des sédiments durant la diagenèse à des températures inférieures à 60 °C. Les conditions de faible température durant la diagenèse concordent avec la préservation de matière organique en abondance dans le shale. [Traduit par la Rédaction]

Introduction

The Macasty shale is an organic-rich black shale in the northern part of the Gulf of St. Lawrence (Fig. 1). It contains abundant graptolites (Riva 1969; McLaughlin et al. 2016), which tightly constrain the deposition of the Macasty shale to the early to mid-Katian stage of the Late Ordovician (453–448 Ma). Continuous subsidence of the area, combined with sea-level rise, led to the deposition of organic-rich Macasty shale within the foreland basin (Malo 2004) (Fig. 2). The deposition of the Macasty shale was contemporaneous with the Taconic orogeny, which involved thrusting of slices of oceanic lithosphere, explosive volcanism, intrusions of dykes and plutons, and metamorphism that affected large areas of eastern North America (van Staal 2005). The tectonic activity was accompanied by the development of sedimentary basins along the Appalachian mountain range (Lavoie 2008) (Fig. 2). Reflecting the dynamic tectonic environments, detritus of sediments in the basins was potentially derived from a variety of sources including Proterozoic Grenville Province and Appalachian allochthons (Comeau et al. 2004).

The location and timing of the development of the Macasty Basin are such that the Macasty shale provides an opportunity to evaluate the depositional setting in the developing Taconic activity during the Late Ordovician. This paper presents the mineralogy; abundances of major, minor, and trace elements; stable isotope compositions; and Sm–Nd isotope data of bulk rock samples and evaluates the provenance and basin setting. To our knowledge, these are the first comprehensive data of inorganic components of the Macasty shale, and they complement large sets of organic geochemical data of the shale by many researchers (e.g., Lavoie et al. 2009, 2016; Dietrich et al. 2011; Chen et al. 2016).

Geological setting

The Anticosti Basin represents the eastern segment of the St. Lawrence platform on the margin of Laurentia (Fig. 2). The western part of the Anticosti Basin is mostly concealed by

Received 12 April 2018. Accepted 28 August 2018.

Paper handled by Guest Editor Thomas Steuber.

K. Hattori, A. Desrochers, and J. Pedro.* Department of Earth and Environmental Sciences, University of Ottawa, Ottawa, ON K1N 6N5, Canada.
Corresponding author: Keiko Hattori (email: khattori@uottawa.ca).
*Current name and address: Janice Botelho, Baker Hughes GE-Sonils Industrial Base, Luanda Boa Vista, Angola.

[1]This paper is part of a Special Issue entitled "Advances in low-temperature geochemistry, diagenesis, and seawater and climate evolution through the Earth's history: a tribute to Jan Veizer".

Fig. 1. (A) Simplified geological map of the study area and (B) A–B cross section showing Lower Ordovician to Lower Silurian strata present below Anticosti Island on the basis of seismic and core correlations. Modified after Castonguay et al. (2007). Oeb, Ellis Bay; Oin, Mingan; Omy, Macasty; Ora, Romaine; Ova, Vauréal; Sbc, Becscie; Scc, Chicotte; Sgu, Gun River; Sju, Jupiter. [Colour online.]

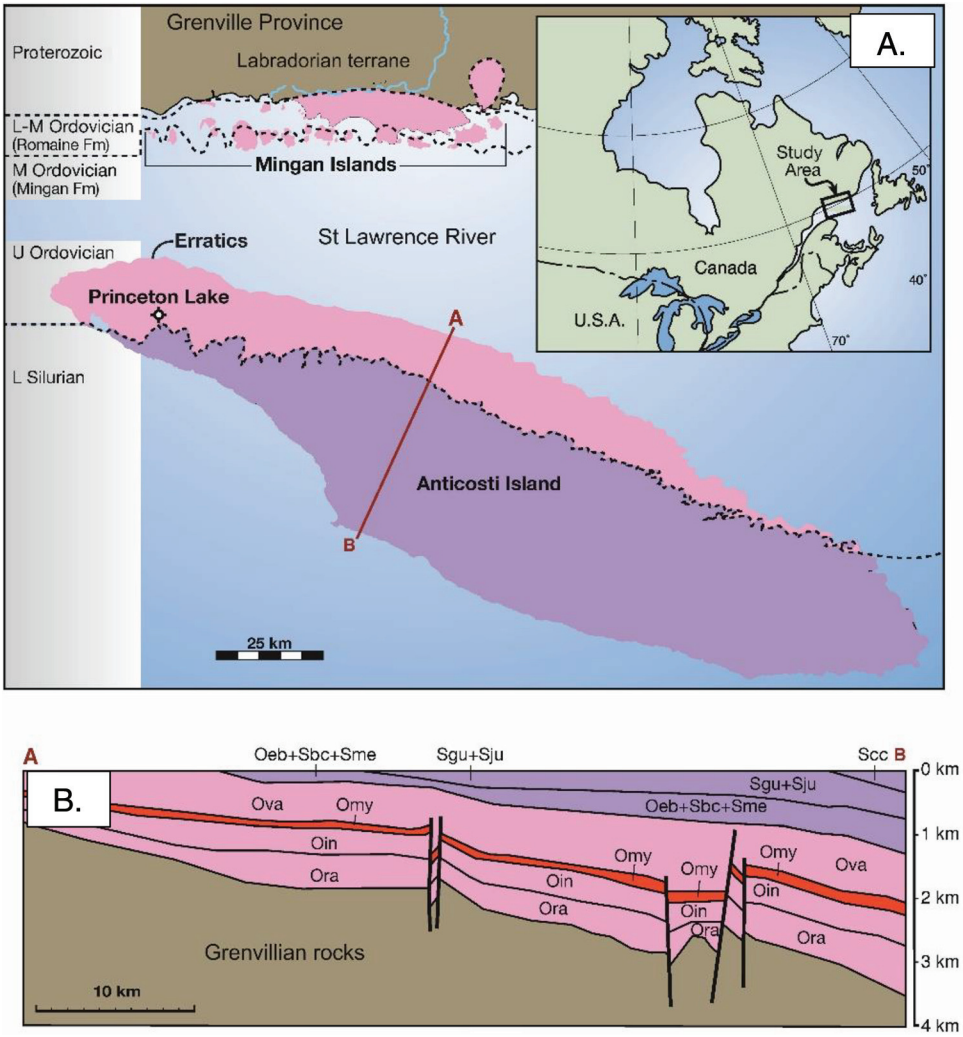

the St. Lawrence River and its adjacent estuary, but the northern part is exposed on the Mingan Islands and Anticosti Island (Fig. 1A). There, the sedimentary rocks record the changes in geological settings. Early Ordovician to early Silurian strata were deposited initially on the Iapetan passive margin of Laurentia and subsequently transformed into a foreland basin in response to the Taconic orogeny (Long 2007; Lavoie 2008). Foreland basin development started with the emplacement of Taconic thrust sheets that were emplaced northwestwards over the northern part of the Gaspé Peninsula and parts of the Gulf of St. Lawrence River (Pinet et al. 2012). Some of the thrust sheets are slices of ocean sediments and mafic igneous rocks of the Iapetus Ocean lithosphere.

The Macasty shale, up to 100 m thick, is present in the subsurface of the western Anticosti Basin (Chen et al. 2016) (Fig. 1). There is no surface exposure of the Macasty shale on Anticosti Island at present, but glacial erratics of the Macasty shale are abundant on the northwest coast of Anticosti Island between English Head and Great Makasti Bay (Schuchert and Twenfofel 1910) (Fig. 1). These glacial erratics were likely eroded from the Macasty shale that was once exposed between the Mingan Islands and Anticosti Island. The outcrops of the Macasty shale are no longer present because they are now submerged below the water of the Jacques Cartier Strait. Well-preserved cephalopods and graptolites are common in the glacial erratics and are identical to those in the subsurface drill core samples in Anticosti Island (Riva 1969). Both erratics and subsurface drill core samples contain abundant graptolites, which are diagnostic of the early to mid-Katian stage biozones of the Late Ordovician (Riva 1969; McLaughlin et al. 2016). The fossil evidence confirms that glacial erratics indeed belong to the Macasty shale.

The Macasty Formation unconformably overlies shallow-water limestone beds of the Mingan Formation (Fig. 1B). The Macasty shale itself shows internal unconformities (Riva 1969; McLaughlin et al. 2016). The presence of several minor unconformities within the Macasty Formation suggests that the shale was deposited in relatively shallow water (Kulkarni et al. 2013). The depositional environment is similar to that of Ordovician and Devonian organic-rich shales in the Appalachian basins of New York State (e.g., Smith and Leone 2010).

Samples

This study uses two types of samples: glacial erratics and drill core samples. Glacial erratics were collected on the northwest shore of Anticosti Island (Fig. 1). Most are slightly rounded and vary in size from 10 to 200 cm. Drill core samples were examined and collected at the Core Library of the Department of Energy and Natural Resources, Québec City. Among them, drill core from Princeton Lake on the northwestern part of Anticosti Island (Fig. 1)

Fig. 2. Late Ordovician paleogeography showing key Laurentian topographic features including emergent highlands, epeiric seas and basins, and rising Taconic mountains. The present-day location of Anticosti Island is shown in red. Present-day state and province boundaries are shown with dashed lines. Modified after McLaughlin and Brett (2007). [Colour online.]

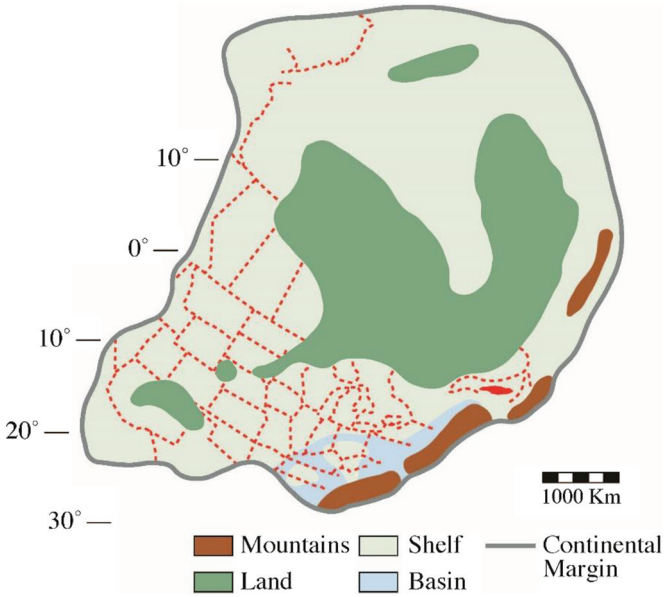

shows 87 m thick Macasty shale from a depth of 912 to 999 m. Because this is one of the thickest sections of the Macasty shale (87 m), the Princeton core samples were used for our detailed geochemical study.

The samples are all clay-sized quartz, feldspars, and sheet silicate minerals with high amounts of calcite, which makes samples fizz with 10% HCl. The fine-grained nature of the rocks and the finely disseminated organic and pyrite give the samples dark gray to black coloration in hand specimens. Marine fossils of cephalopods and graptolites are abundant in both erratics and drill core samples. The remnants of radiolarian tests are locally abundant in thin sections. Pyrite grains are recognized under a binocular microscope in most specimens. Small (≤0.1 mm) metallic cubes of pyrite are present along fractures and bedding planes. Thin-section examination shows common occurrences of framboidal grains of pyrite.

Analytical methods

The rock samples were washed with distilled water, then dried quickly using pressurized air. The samples were crushed with a jaw crusher and pulverized for geochemical analysis using a ceramic disc.

Approximately 1 g of rock powder was placed in an oven at 110 °C for >8 h to measure $H_2O(-)$. The values of $H_2O(-)$ are less than 0.1 wt.%. The power was subjected to a stepwise heating to measure the loss on ignition (LOI) following the method of Heiri et al. (2001), which involved heating samples at 550 °C for 6 h (LOI-550 °C) and 1050 °C for 2 h (LOI-1050 °C). The value of LOI-550 °C is considered to be the abundance of organic matter and that of LOI-1050 °C represents the amounts of CO_2 from carbonate. Heiri et al. (2001) reported that the organic material burns quickly and releases CO_2 in the first 2 h, but the combustion may not be complete even after 24 h. We chose 6 h of heating time because the loss was small, <0.3%, after 6 h of heating. Heiri et al. (2001) suggested 900 °C for 2 h for the measurement of carbonate, but we found that the duration of heating and the temperature were not sufficient to release all the CO_2 from the carbonate. Therefore, we chose 1050 °C of heating for 2 h to complete the release of H_2O and CO_2 from the samples.

The abundances of major, minor, and trace elements were determined on the sample powder after baking at 1050 °C and are listed in Table 1. The reported abundances of elements are all volatile free. Major element analysis used a Philips PW 2400 X-ray fluorescent spectrometer at the University of Ottawa after fusing the bulk rock powder with a flux composed of 78.5% $Li_2B_4O_7$ and 21.5% $LiBO_2$. Trace element abundances were determined with an inductively coupled plasma – optical emission spectrometer and an inductively coupled plasma – mass spectrometer after digestion of samples with a mixture of HCl, HNO_3, $HClO_4$, and HF (analytical code, Ultratrace 4) at Activation Laboratories (Ancaster, ON, Canada). The concentrations of Nd and Sm were determined with an isotope dilution technique using a solution enriched in ^{148}Nd and ^{149}Sm.

Carbon and oxygen isotope compositions of calcite were determined by a conventional technique using 100% orthophosphoric acid at 25 °C. CO_2 released from another aliquot of powdered samples was introduced to a Thermo Finnigan Delta XP mass spectrometer. Calcite contents are high in all samples (Table 1). Therefore, no attempt was made to physically separate calcite for the isotope analysis. Analytical precision is ±0.1‰ on the basis of duplicate analysis of samples and repeated analysis of internal working reference calcite. Both isotope compositions are expressed in per mil notation relative to Pee Dee Belemnite (PDB) (Table 2).

Sulfur isotope composition for sulfur in disseminated fine-grained pyrite was determined after digesting samples in a mixture of conc HNO_3-HBr (Seastar Chemical) at 120 °C and was converted to $BaSO_4$ by adding 10% $BaCl_2$ solution. Coarse-grained pyrite cubes were hand picked under a binocular microscope. Samples were ground and mixed with tungsten oxide in an Sn capsule and were combusted at 1800 °C in the Vario EL elemental analyzer. SO_2 released from a sample was separated from other gases and introduced to the Thermo Finnigan XP isotope ratio mass spectrometer in the J. Veizer Isotope Laboratory at the University of Ottawa, and S isotope compositions of samples are listed in Table 2. Duplicate analysis of samples and laboratory in-house working references shows a precision of ±0.2‰.

For Nd isotope analysis, ~50 mg of samples was dissolved in an HF-HNO_3 mixture at 180 °C overnight; HNO_3 was then added, and finally, HCl, following dryness in between steps. Light rare earth elements (REE) were separated by a routine procedure using an alkali resin (Bio-Rad AG50W, 100 mesh) followed by the separation of Nd and Sm using the Ln resin from Eichrom Technologies Inc. Neodymium was eluted using 0.26 N HCl. Samples were loaded with H_3PO_4 on one side of a Re double filament and run at temperatures of about 1700–1800 °C with a thermal ionization mass spectrometer, the Thermo Finnigan Triton. The sample preparation was carried out at the Department of Earth Sciences at the University of Ottawa, and mass spectrometry was conducted at Carleton University in Ottawa. Digestion and analysis of United States Geological Survey reference BCR-2 during the analysis of samples yielded $^{143}Nd/^{144}Nd = 0.512640 \pm 14$ ($n = 2$). The mass spectrometer condition was verified by running a working Nd standard solution ($^{143}Nd/^{144}Nd = 0.511823–0.511837$) at the beginning of each analytical session, and the solution was calibrated with La Jolla standard (0.511855 ± 9).

All rock samples contain calcite and organic matter, both of which may contain significant amounts of light REE. Because calcite formed during the diagenesis, Nd in calcite may have different isotopic compositions from those of Nd in detritus. Furthermore, Nd in organic matter may have been mobile and introduced to the rocks during the diagenesis or after the lithification. To make sure that measured Nd belongs to the detritus of the rocks, three samples were washed with 10% HCl for several minutes to remove calcite, baked at 1050 °C, and washed to remove calcite

Table 1. Bulk rock compositions.

Sample	Core depth (m)	LOI-500 (%)	LOI-1050 (%)	SiO_2 (%)	TiO_2 (%)	Al_2O_3 (%)	$Fe_2O_3(T)$ (%)	CaO (%)	K_2O (%)	MgO (%)	MnO (%)	Na_2O (%)	P_2O_5 (%)	S (%)	$\delta^{34}S$ (‰)	V (ppm)
Vauréal Formation																
M228		nd	nd	48.33	0.63	13.34	6.46	19.81	2.23	5.32	0.14	0.93	0.10	nd	nd	98
M225	894.57	0.80	22.6	42.24	0.44	8.75	4.36	33.48	1.84	3.41	0.18	0.83	0.11	nd	nd	63
M223	897.31	1.72	20.3	47.11	0.56	10.96	4.95	28.08	2.40	4.66	0.18	0.98	0.11	nd	nd	77
M221	900.36	1.30	28.9	30.36	0.40	7.84	3.90	46.06	0.85	4.29	0.18	0.65	0.17	nd	nd	46
M220	902.19	2.17	23.4	39.57	0.49	10.12	4.45	34.52	1.92	4.18	0.23	0.86	0.13	nd	nd	77
M219	903.41	1.70	16.7	48.50	0.64	14.07	5.89	19.48	3.41	5.06	0.16	0.68	0.16	nd	nd	112
M217	906.46	1.60	29.7	29.24	0.38	8.09	3.22	53.88	1.14	2.94	0.47	0.54	0.10	nd	nd	57
Macasty Formation																
AC1	Erratics	nd	18.1	69.51	0.40	8.62	3.82	12.98	1.99	1.58	0.05	0.83	0.23	1.74	0.1	212
AC2	Erratics	nd	15.7	73.46	0.45	9.41	4.10	7.70	2.27	1.62	0.04	0.80	0.15	1.59	−2.2	227
AC3	Erratics	nd	16.0	72.40	0.45	9.46	5.00	7.76	2.29	1.59	0.04	0.84	0.14	1.68	−0.2	218
AC4	Erratics	nd	16.4	73.30	0.45	9.43	3.56	8.43	2.28	1.51	0.03	0.88	0.14	1.43	−1.7	170
AC5	Erratics	nd	19.2	68.21	0.43	9.21	3.35	13.92	2.27	1.52	0.04	0.82	0.22	1.28	−0.9	236
AC6	Erratics	nd	15.6	75.31	0.36	7.98	3.41	8.85	1.93	1.37	0.03	0.63	0.13	1.15	−1.1	175
AC7	Erratics	nd	15.1	75.57	0.36	8.08	3.25	8.50	1.96	1.42	0.03	0.70	0.13	1.58	−2.4	221
AC8	Erratics	nd	16.0	73.48	0.45	9.43	3.92	7.83	2.30	1.60	0.04	0.82	0.15	1.32	−1.5	173
M216	907.99	1.39	29.4	31.58	0.39	8.23	3.68	49.40	0.65	4.46	0.91	0.63	0.11			50
M212	914.09	5.93	11.5	59.30	0.66	12.60	4.90	14.44	2.70	1.71	0.06	1.62	0.19	1.48	−3.6	179
M210	917.00	4.29	15.0	59.05	0.43	9.16	3.54	20.88	1.77	1.77	0.06	1.10	0.20	1.25	−2.9	154
M208	920.49	6.79	11.1	64.94	0.47	9.47	3.67	14.88	1.98	1.42	0.04	1.22	0.22	2.84	−2.3	167
M206	924.00	5.76	9.8	72.50	0.36	6.58	2.53	13.02	1.32	1.19	0.03	0.97	0.14	1.65	−5.0	136
M205	925.00	4.21	19.0	53.62	0.34	6.52	3.95	27.86	1.18	1.50	0.05	0.88	0.17	1.42	0.9	129
M204	927.00	3.94	21.8	51.61	0.27	5.47	3.27	35.95	0.81	1.66	0.07	0.63	0.26	nd	nd	126
M203	927.81	3.81	21.2	50.03	0.30	5.98	4.29	32.55	1.02	1.42	0.06	0.77	0.21	nd	nd	123
M200	932.69	6.68	12.7	64.11	0.43	8.66	3.59	16.45	1.76	1.92	0.04	0.99	0.21	1.16	−10.6	151
M199	933.91	8.23	12.4	63.37	0.44	9.27	4.09	15.99	1.84	1.92	0.04	1.15	0.23	1.53	−3.9	227
M195	940.32	7.65	6.3	72.03	0.46	10.07	3.88	6.68	2.11	1.30	0.03	1.20	0.14	1.58	−0.2	191
M194	941.84	6.26	8.4	69.55	0.44	10.10	4.07	9.10	2.17	1.78	0.03	1.06	0.16	1.47	0.2	206
M193	943.37	6.08	11.9	65.11	0.42	9.17	3.61	14.90	1.91	1.96	0.04	1.05	0.18	1.25	−3.3	174
M190	948.25	1.80	34.2	26.44	0.17	3.48	3.03	64.59	0.25	1.35	0.17	0.35	0.17	nd	nd	77
M186	952.52	6.20	10.5	65.87	0.48	10.35	3.93	12.82	2.29	1.69	0.03	1.08	0.16	1.61	−7.4	198
M181	959.53	2.41	24.6	46.66	0.23	4.97	3.36	41.67	0.85	1.55	0.05	0.55	0.12	nd	nd	95
M180	960.75	4.55	11.4	65.86	0.44	9.39	3.62	14.42	2.06	2.10	0.04	0.97	0.15	1.28	−3.5	164
M175	968.38	1.91	26.3	43.14	0.22	5.00	2.87	45.82	0.82	1.53	0.04	0.46	0.10	nd	nd	81
M174	969.90	1.80	28.7	38.99	0.22	4.77	2.81	49.91	0.70	2.04	0.04	0.39	0.12	nd	nd	85
M172	972.95	nd	nd	30.12	0.21	4.61	2.67	59.68	0.51	1.77	0.04	0.30	0.08	nd	nd	64
M171	974.00	4.98	12.2	55.97	0.59	13.16	5.81	14.05	3.22	3.09	0.05	0.89	0.19	2.24	2.6	183
M170	976.00	1.69	32.3	27.54	0.22	5.00	3.06	61.46	0.71	1.59	0.04	0.26	0.10	nd	nd	73
M168	979.05	2.00	28.5	37.80	0.20	4.88	3.03	50.92	0.85	1.76	0.05	0.40	0.12	nd	nd	65
M165	983.63	5.80	11.4	62.50	0.46	11.00	5.28	13.50	2.65	2.21	0.04	0.85	0.15	2.24	−3.9	157
M163	988.20	2.69	26.8	40.97	0.21	4.87	3.10	47.96	0.67	1.42	0.05	0.60	0.15	nd	nd	62
M161	990.64	4.08	17.1	54.41	0.36	8.70	3.77	25.00	1.86	1.61	0.05	0.64	0.155	1.51	−4.0	90
M159	993.69	3.31	26.7	34.93	0.26	6.45	2.76	44.87	1.28	1.38	0.06	0.49	0.129	nd	nd	71

Note: LOI, loss on ignition; nd, not determined.

and possible Nd in organic matter. The Nd isotope compositions of these acid-baked samples were compared with those of nontreated samples. The concentrations of Nd and Sm for these samples were lower than those for the nontreated samples, but the isotope compositions of Nd were very similar to those of the nontreated samples in analytical uncertainty (Table 3), indicating that the measured Nd isotope values represent those of the detritus components of the samples.

Mineral phases were examined on selected powdered samples using a Phillips PW 3020 X'Pert X-ray diffractometer (XRD), using a Cu anode tube with a scan speed of 0.25°/min, at the X-ray Laboratories of the University of Ottawa. The patterns of XRD were compared in samples before and after 10% HCl treatment.

Results

Mineralogy

Thin sections showed white mica, calcite, organic matter, quartz, and minute grains of framboidal pyrite disseminated throughout the samples. XRD patterns of bulk rock samples confirm the presence of these minerals plus minor kaolinite.

Bulk rock compositions

The mineralogy is consistent with the major element abundances of bulk rocks. The concentrations of SiO_2 are broadly correlated with those of TiO_2 (Fig. 3A). Because TiO_2 is not soluble in aqueous solutions at low temperatures, the broad positive correlation of the two elements suggests a predominantly detrital origin of SiO_2. The slight elevation of SiO_2, 68–75 wt.%, for glacial erratics is explained by an abundance of radiolarian tests in these samples. The occurrences of skeletons in thin sections suggest that SiO_2 was likely leached from the fossil tests to form the silica cement of the rocks. SiO_2 forms clay-sized fine material and does not form veinlets or fracture fills, suggesting that this silica leaching from radiolarian tests and deposition and dissemination likely took place during the very early stage of diagenesis of the Macasty shale. High SiO_2 contents likely kept these rocks intact, physically hard, and resistant to fragmentation during erosion

Ba (ppm)	Rb (ppm)	Sr (ppm)	Zr (ppm)	Cr (ppm)	La (ppm)	Ce (ppm)	Pr (ppm)	Nd (ppm)	Sm (ppm)	Eu (ppm)	Gd (ppm)	Dy (ppm)	Ho (ppm)	Er (ppm)	Yb (ppm)	Y (ppm)
546	78	648	140	58	nd	nd	nd	nd	nd	nd	nd	nd	nd	nd	nd	nd
1037	63	830	252	38	nd	nd	nd	nd	nd	nd	nd	nd	nd	nd	nd	nd
1431	84	767	180	49	24	49	5.6	20	3.52	1.13	3.41	2.7	0.62	1.6	1.5	17
320	31	1220	133	39	nd	nd	nd	nd	nd	nd	nd	nd	nd	nd	nd	nd
478	65	929	80	42	nd	nd	nd	nd	nd	nd	nd	nd	nd	nd	nd	nd
613	127	619	130	65	nd	nd	nd	nd	nd	nd	nd	nd	nd	nd	nd	nd
523	37	769	56	31	nd	nd	nd	nd	nd	nd	nd	nd	nd	nd	nd	nd
188	67	380	84	64	26.2	49.6	6.0	21.9	4.3	1.0	4.4	3.7	0.84	2.2	2.04	1.0
196	84	266	80	72	24.6	49.5	6.1	21.7	4.1	0.9	3.8	3.4	0.7	2.0	1.75	0.9
212	82	250	83	64	24.7	49.1	5.9	20.9	4.2	0.9	4.0	3.3	0.71	1.9	1.9	0.9
180	72	371	87	74	20.6	41.5	5.0	19.0	3.7	0.8	3.6	3.0	0.6	1.8	1.68	0.8
300	90	939	104	71	28.8	54.0	6.7	23.3	4.6	1.0	4.4	3.8	0.85	2.4	2.18	1.0
177	71	250	68	57	22.4	44.2	5.3	18.4	3.6	0.8	3.2	2.9	0.57	1.7	1.61	0.8
217	80	233	69	70	23.5	46.8	5.7	20.6	3.9	0.8	3.8	3.3	0.7	1.9	1.74	0.8
197	67	221	76	60	21.7	43.1	4.9	19.6	3.8	0.8	3.7	3.1	0.6	1.8	1.56	0.8
233	22	1040	112	33	nd	nd	nd	nd	nd	nd	nd	nd	nd	nd	nd	nd
468	101	921	107	74	26.9	54.5	6.3	22.7	4.1	0.94	3.9	3.4	0.7	2	1.7	22.4
554	58	1140	130	52	nd	nd	nd	nd	nd	nd	nd	nd	nd	nd	nd	nd
573	73	1020	87	61	25.9	49.9	5.7	20.3	3.7	0.89	3.9	3.1	0.7	1.9	1.6	22.4
442	50	837	64	45	19.6	37.9	4.5	16.4	3.5	0.6	4.2	3.7	0.8	2.2	1.9	22.7
437	38	1120	53	35	16.7	30.7	3.5	12.9	2.5	0.64	2.8	2.3	0.5	1.4	1.2	17.5
433	21	1240	36	30	nd	nd	nd	nd	nd	nd	nd	nd	nd	nd	nd	nd
301	38	1280	115	32	nd	nd	nd	nd	nd	nd	nd	nd	nd	nd	nd	nd
519	62	1380	61	57	20.3	37.8	4.4	16.2	3.1	0.76	3.6	2.9	0.6	1.7	1.5	20.6
552	63	1390	71	67	20.9	38.9	4.5	16.7	3.2	0.8	3.7	3.2	0.7	1.9	1.6	21.7
430	76	680	66	76	20.2	41.3	4.8	17.5	3.3	0.77	3.3	2.8	0.6	1.6	1.3	18.2
726	80	879	107	70	21.2	42.7	5	18.5	3.5	0.86	3.7	3.1	0.6	1.9	1.6	21
602	67	1390	131	63	22	42.4	4.7	17.2	3.2	0.84	3.7	3.1	0.6	1.9	1.5	21.8
296	2	1270	90	16	nd	nd	nd	nd	nd	nd	nd	nd	nd	nd	nd	nd
639	79	1380	141	68	22.4	44.3	5.1	18.6	3.5	0.84	3.8	3.1	0.6	1.8	1.5	18.8
399	21	984	90	24	nd	nd	nd	nd	nd	nd	nd	nd	nd	nd	nd	nd
940	73	1180	137	66	22.6	45.7	5.3	19.4	3.5	0.83	3.4	3.1	0.6	1.8	1.6	20.9
881	29	703	72	20	nd	nd	nd	nd	nd	nd	nd	nd	nd	nd	nd	nd
874	21	1030	85	104	nd	nd	nd	nd	nd	nd	nd	nd	nd	nd	nd	nd
687	12	914	81	16	nd	nd	nd	nd	nd	nd	nd	nd	nd	nd	nd	nd
832	117	549	107	81	28.4	55.8	6.2	22.6	4.1	1	4.2	3	0.7	1.8	1.6	20.2
253	22	875	82	25	nd	nd	nd	nd	nd	nd	nd	nd	nd	nd	nd	nd
357	26	634	75	21	nd	nd	nd	nd	nd	nd	nd	nd	nd	nd	nd	nd
442	94	497	102	64	25.5	52.8	5.9	21.7	4	0.94	3.9	3.2	0.7	1.9	1.7	21.5
451	18	800	72	17	nd	nd	nd	nd	nd	nd	nd	nd	nd	nd	nd	nd
363	59	534	65	44	nd	nd	nd	nd	nd	nd	nd	nd	nd	nd	nd	nd
254	49	505	66	32	nd	nd	nd	nd	nd	nd	nd	nd	nd	nd	nd	nd

and subsequent glacial transport. The brittle parts of shale, which are common in drill core samples, were more easily disintegrated during the glacial processes.

The weight ratios of Th/U vary from 0.3 to 0.99 for the Macasty shale (Fig. 4). The glacial erratics show consistently low ratios of around 0.3. The values are much lower than those for common sedimentary rocks. For example, the value for the North American Shale Composite (NASC) is 4.6 (Condie 1993; Fig. 4), and that for the upper continental crust is 3.8 (Taylor and McLennan 1985; Rudnick and Gao 2004). The low Th/U values result from enrichment in U in the Macasty shale. Uranium is a redox-sensitive element and is highly mobile as U^{6+} in oxygenated water and fixed as U^{4+} in reduced conditions. The low values of Th/U from the Macasty shale attest to the anoxic conditions that prevailed during the deposition. It should be noted that the overlying Vauréal Formation shows high Th/U, ~3.7, which is similar to that of many siliciclastic sedimentary rocks deposited under oxidizing conditions (Fig. 4). The change in the values reflects the different depositional environments of the Macasty and Vauréal formations.

The bulk rocks contain low concentrations of elements associated with mafic-ultramafic igneous rocks. For example, Cr contents vary from 14 to 81 ppm, which are much lower values than the value of 125 ppm for the NASC by Condie 1993 and an average of 92 ppm Cr for the upper continental crust (Rudnick and Gao 2004). The data suggest very little contribution of mafic-ultramafic rocks to the Macasty shale. Furthermore, Zr contents are high. The average Zr/Cr ratio for the Macasty samples is 2.5 ± 1.4 (1σ), which is higher than 1.6 for NASC (Condie 1993) and 2.0 for the upper continental crust (Rudnick and Gao 2004). The data are consistent with overall felsic rocks being the source of terrigenous detritus.

The abundances of REE normalized to NASC by Haskin and Haskin (1966) show a near flat pattern near 1 and are very similar among all samples, with the exception of one with low Eu (Fig. 5). Negative anomalies of Eu in igneous rocks develop during the fractional crystallization of plagioclase. Therefore, highly evolved granitic rocks commonly show low Eu. This particular sample from the core likely had a high contribution of such evolved

Table 2. Carbon and oxygen isotope compositions of calcite.

Sample	Core depth (m)	$\delta^{13}C_{PDB}$ (‰)	$\delta^{18}O_{PDB}$ (‰)	Temp. (°C)[a]	Temp. (°C)[b]
Vauréal Formation					
M225	894.57	0.7	−5.0	41	21
M223	897.31	0.5	−4.7	40	20
M221	900.36	0.3	−5.2	42	23
M220	902.19	0.4	−5.2	42	22
M217	906.46	−1.0	−4.1	36	16
Macasty Formation					
M216	907.99	−1.5	−5.2	42	22
M204	926.59	−2.0	−7.2	54	34
M203	927.81	−2.2	−7.2	54	34
M190	948.25	−0.8	−5.7	45	25
M181	959.53	−1.2	−6.2	48	28
M175	968.38	−0.4	−5.9	46	26
M174	969.90	−0.2	−6.4	49	29
M172	972.95	0.3	−6.4	49	29
M170	976.00	−0.1	−6.4	49	29
M168	979.05	0.1	−5.8	46	26
M167	980.58	−0.1	−6.3	49	29
M163B	986.68	−0.2	−6.6	50	30
M163A	988.20	0.0	−6.6	50	30
M160	992.17	0.4	−6.6	50	31
M159	993.69	0.6	−5.6	45	25
M158	995.22	0.0	−6.8	51	31

Note: PDB, Pee Dee Belemnite.

[a]Assuming crystallization from sea water with $\sigma^{18}O = 0‰$, using the equation: Temp. (°C) = 16.0 − 4.2(δc − δw) + 0.13[(δc − δw)]² (Faure 1986).

[b]Assuming crystallization from sea water with s18O = −4‰, using the same equation as in footnote *a*.

Table 3. Neodymium isotope compositions.

Sample[a]	Core depth (m)	Nd (ppm)	Sm (ppm)	$^{143}Nd/^{144}Nd$	εNd (present)	$^{147}Sm/^{143}Nd$	$^{143}Nd/^{144}Nd$ (450 Ma)	εNd(*t*) (450 Ma)	*T* Nd (CHUR) (Ga)	*T* Nd (DM) (Ga)	*T* Nd (continent)[b] (Ga)
Vauréal Formation											
M219	903.41	29.90	5.43	0.511805	−16.3	0.1098	0.511481	−11.3	1.46	1.93	1.78
M219A	903.41	26.19	4.80	0.511813	−16.1	0.1109	0.511486	−11.2	1.46	1.93	1.78
Macasty Formation											
AC-1	Erratics	18.49	3.17	0.511974	−12.9	0.1035	0.511669	−7.6	1.09	1.56	1.44
AC-2	Erratics	18.01	3.45	0.511974	−12.9	0.1158	0.511633	−8.3	1.25	1.78	1.62
AC-3	Erratics	17.42	3.40	0.511974	−12.9	0.1179	0.511627	−8.4	1.28	1.82	1.66
AC-4	Erratics	16.99	3.74	0.511974	−12.9	0.1330	0.511583	−9.3	1.58	2.15	1.97
M216	907.99	17.64	3.32	0.511910	−14.2	0.1139	0.511574	−9.5	1.34	1.85	1.69
M208	920.49	22.98	4.32	0.511984	−12.8	0.1138	0.511649	−8.0	1.20	1.74	1.58
M194A*	941.84	18.84	3.69	0.511937	−13.7	0.1184	0.511588	−9.2	1.36	1.89	1.73
M194	941.84	23.01	4.49	0.511929	−13.8	0.1179	0.511582	−9.3	1.37	1.89	1.73
M175A*	968.38	14.44	2.70	0.511869	−15.0	0.1131	0.511535	−10.2	1.40	1.89	1.75
M175	968.38	18.72	3.51	0.511868	−15.0	0.1134	0.511534	−10.2	1.41	1.90	1.74
M165F	974.00	21.60	4.14	0.511751	−17.3	0.1160	0.511410	−12.7	1.67	2.13	1.98
M165	983.63	26.91	5.14	0.511750	−17.3	0.1155	0.511409	−12.7	1.66	2.12	1.97
M158F	995.22	17.01	3.24	0.511768	−17.0	0.1150	0.511429	−12.3	1.62	2.08	1.93

Note: CHUR, chondritic uniform reservoir; DM, depleted mantle.

[a]Sample numbers with A are acid treated and washed.

[b]Model age calculated on the basis of εNd(0) = 7.2 for a "new continent" (see text).

rocks. The data suggest a stable supply of terrigenous material from the granitic source rocks to the Anticosti Basin during the deposition of the Macasty shale, without a significant change.

Nd isotope compositions

Neodymium isotope compositions of bulk rocks were measured for glacial erratics and drill core samples. The values of $^{143}Nd/^{144}Nd$ are calculated at 450 Ma and presented as εNd(*t*), where $\varepsilon Nd(t) = [(^{143}Nd/^{144}Nd)_s/(^{143}Nd/^{144}Nd)_{CHUR} - 1]*10\,000$, where $(^{143}Nd/^{144}Nd)_S$ and $(^{143}Nd/^{144}Nd)_{CHUR}$ are the ratios of a sample and chondritic uniform reservoir (CHUR) value at 450 Ma. The values for εNd(*t*) for samples are all low, ranging from −7.6 to −12.7 (Table 3; Fig. 6). The values for the deeper part of the Macasty Formation show low values compared with those of the upper parts (Table 3). Crustal residence ages were calculated using the bulk silicate earth (T_{CHUR}), depleted mantle (T_{DM}), using the depleted mantle value of Workman and Hart (2005), and "new continent" model ages. The continent model age is based on the Hf isotope composition (εHf(0) = 13.2) of a new continent proposed by Dhuime et al. (2011). This is translated into εNd(0) = 7.2 using the Nd and Hf isotope positive correlation by Workman and Hart (2005). Crustal residence ages of samples give Proterozoic ages (Fig. 6). When sediments have different provenances, crustal residence ages are weighted averages of mixed provenances, and the ages are not necessarily related to the real ages of the source rocks. Furthermore, igneous rocks may show old crustal residence ages when they extensively assimilate ancient rocks. For the Macasty shale, it

Fig. 3. (A) SiO_2 versus TiO_2 and (B) V versus K_2O of bulk rock compositions for the Macasty shale compared with the values for the overlying Vauréal Formation, and North American Shale Composite (NASC; Condie 1993) and average composition of the upper continental crust (UC; Rudnick and Gao 2004). Overall positive correlation between SiO_2 and TiO_2 suggests detrital origin of SiO_2. Vanadium is +3 under reduced conditions to be incorporated into the Al site of illite. The broad positive correlation between K_2O and V supports this interpretation. [Colour online.]

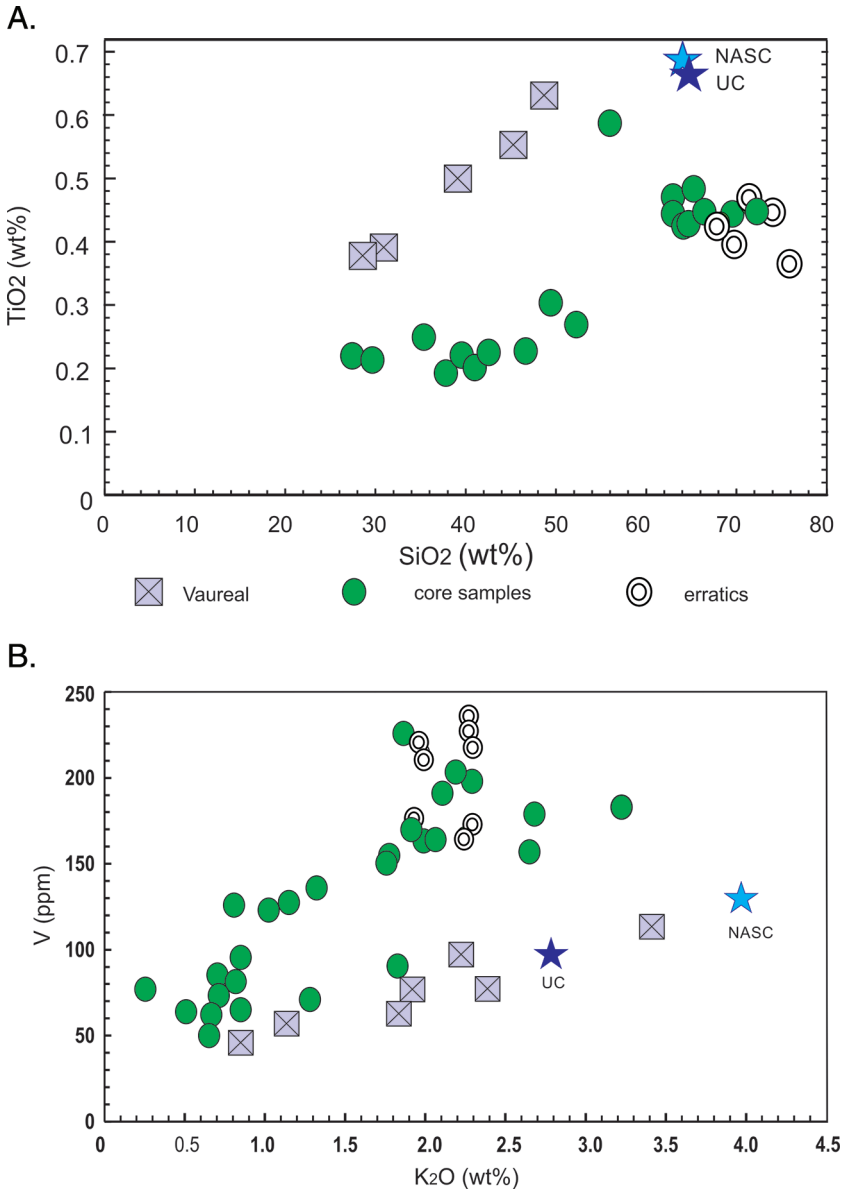

is reasonable to consider Proterozoic Grenvillian rocks as the predominant source, considering the location of the basin.

Sulfur isotope compositions of pyrite

Sulfur may be incorporated into organic matter (Chukhrov et al. 1980), but the isotope compositions and the abundances of sulfur reported in Table 1 are most likely those of pyrite because pyrite is abundant in hand specimens and thin sections. Furthermore, a mixture of concentrated HNO_3-HBr was used to extract sulfur for the measurement. Extraction of sulfur bound in organic matter usually requires more aggressive extraction after the fusion of samples with a flux or the use of a Parr bomb. Therefore, the reported contents of sulfur and its isotope compositions are considered to represent those of sulfur in fine-grained pyrite disseminated within the samples.

The sulfide sulfur contents are positively correlated with the organic carbon content (Fig. 7A) and total Fe (Fig. 7B), as observed in many organic-rich sediments (e.g., Berner and Raiswell 1983; Lyons and Berner 1992). The data from the Macasty shale are consistent with the active role of organic matter and Fe for the fixation of sulfide sulfur in the sediments.

The values of $\delta^{34}S$ for fine-grained pyrite are similar –2.5‰ ± 2.7‰, excluding one outlier value of –10.6‰ (Table 1). The values of $\delta^{34}S$ for coarse-grained pyrite that is hand picked from bedding planes and fractures are high overall and vary from +2.7‰ to +28.1‰ (Table 4). The values are different even within a single hand specimen. Samples M178 and M197 contain cubes of pyrite on bedding planes, and different grains were subjected to sulfur isotope analysis. Different pyrite grains yielded different isotope compositions (Table 4), suggesting highly heterogeneous S-isotope compositions of coarse-grained pyrite. The evidence reflects different generations of pyrite along fractures and bedding planes.

Carbon isotope compositions

The values of $\delta^{13}C$ for calcite show a narrow range, from –2.2‰ to +0.6‰ (Table 2), similar to the modern marine carbonate value

Fig. 4. Vertical variations of bulk rock compositions for the Macasty shale in the drill core samples, compared with those of glacial erratics and North American Shale Composite (NASC). The Macasty shale overlies limestone beds of the Mingan Formation (shown as limestone pattern at the base of the stratigraphic column). (A) CaO, P_2O_5, and CO_2; (B) chemical index of alteration (CIA) and Th/U. The values for CO_2 are the loss on ignition values at 1050 °C for 2 h after baking the samples at 550 °C for 6 h to burn organics. The value of CIA gives a measure of the degree of weathering (e.g., Nesbitt and Young 1982). It is expressed as % and is defined as molecular proportions of major elements, $(Al_2O_3/[Al_2O_3 + CaO^* + Na_2O + K_2O]) \times 100$, where CaO* is the silicate fraction. In our samples, CaO* is 0 because CaO is almost all in calcite. NASC values are from Condie (1993). The weight ratios of Th/U for the NASC (4.6) and those for the Vauréal Formation (~3.7) are far higher than those for the Macasty shale. UCC, upper continental crust. [Colour online.]

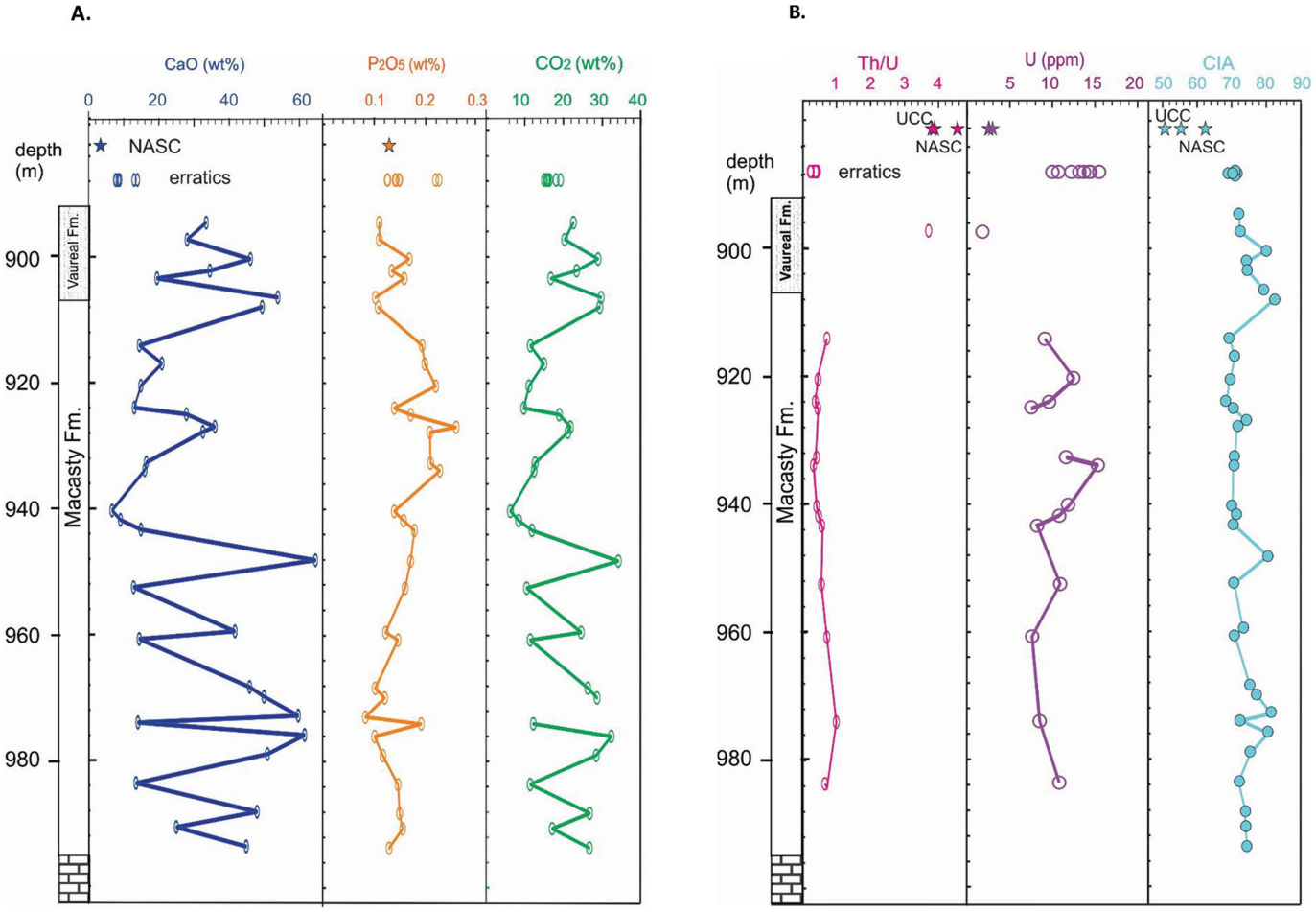

Fig. 5. Rare earth element abundances of Macasty shale samples normalized to the values of North American Shale Composite (NASC), which are compiled by Haskin and Haskin (1966). The not-smooth line is mostly a result of varying contents of Eu, reflecting the different degrees of evolved granitic rocks in the provenance. [Colour online.]

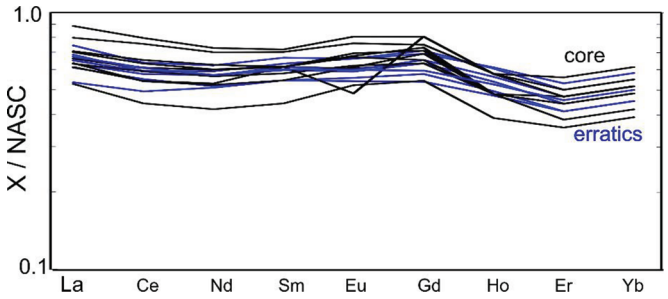

of 0‰ and to average early to mid-Katian values derived from well-preserved brachiopods (Shields et al. 2003). $\delta^{18}O_{PDB}$ values for calcite in our samples range from –7.2‰ to –5.0‰ (Table 2), which are lower than those expected for its crystallization at the depositional site from seawater.

Isotope compositions of organic carbon were measured for glacial erratics. They show a significant variation, from –24‰ to –29‰ (Table 5). The values are lower than those for most present-day marine organic matter (–18‰ to –23‰) but are similar to those for coastal sediments, such as those in the Adriatic Sea (–21‰ to 30‰; Ogrinc et al. 2005).

Discussion

Mineralogy

The rocks are very fine grained, and it is impossible to identify all minerals in thin sections under a petrographic microscope. Although XRD patterns were examined, minerals with an abundance of <10% commonly do not show discernable X-ray peaks. Therefore, bulk chemical compositions are used to verify the mineralogy of rocks. The weight ratios of Al_2O_3/K_2O vary from 4.0 to 7.3 in the Macasty shale. The values are much higher than that of illite, ~2.3–2.5. This is consistent with the occurrence of kaolinite in the XRD pattern. This is also apparent in the ternary plot of $Al_2O_3 – (Na_2O + CaO^*) – K_2O$ (Fig. 8). The samples plot closer to the Al_2O_3 apex than to the position of illite in the diagram, indicating the presence of kaolinite. The presence of kaolinite in the Macasty shale suggests that it was brought to the site as a detrital mineral,

Fig. 6. Neodymium isotope evolution of the Macasty shale (black lines). Depleted mantle value is after Workman and Hart (2005). Crustal residence ages (in Ga) for the Macasty shale are calculated on the basis of chondritic uniform reservoir (CHUR), "continent" composition, and depleted mantle (DM), and the ages are shown as thick bars. "Continent" formation age is calculated using $^{143}Nd/^{144}Nd = 0.513005$ ($\varepsilon Nd = 7.2$) for a "new continent" on the basis of $\varepsilon Hf = 13.2$ as proposed by Dhuime et al. (2011) and the positive relationship between Nd and Hf isotope compositions in the mantle as proposed by Workman and Hart (2005). [Colour online.]

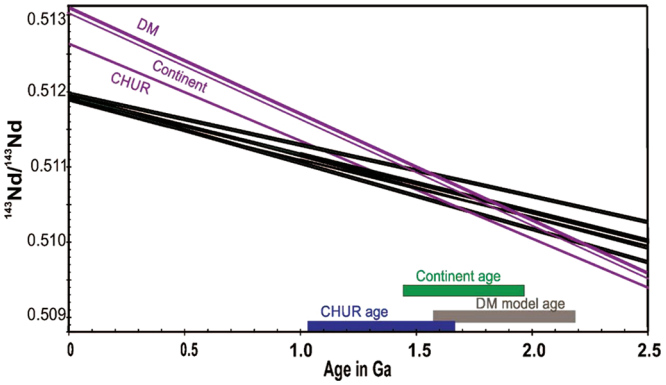

Fig. 7. (A) Concentrations of sulphur and organic carbon in wt.%. The dashed line is for the relationship between sulphide sulphur and organic carbon in normal marine sediments formed under oxic conditions (Lyons 1997). (B) Plot of total Fe against sulphur for the Mascasty shale. The thin dotted line shows the correlation of the two elements for pyrite and the dashed line shows the correlation of the two elements commonly observed in euxinic sediments (Jenkyns 1988). [Colour online.]

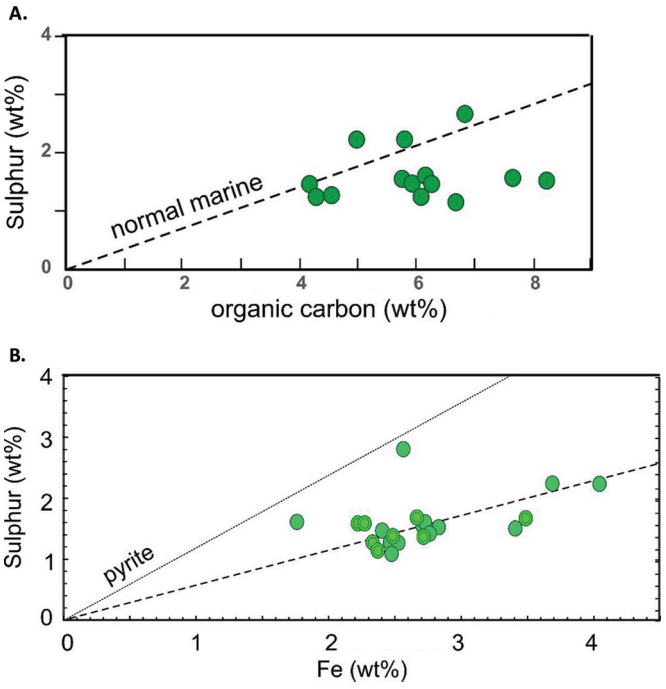

because kaolinite cannot be formed during deposition in alkaline seawater. Furthermore, kaolinite could not be formed during the diagenesis of rocks when abundant calcite crystallized.

CaO contents on a volatile-free basis vary significantly, from 6.7 to 56.0 wt.%, but P_2O_5 contents remain low, ranging from 0.08 to 0.25 wt.% (Fig. 4). The data suggest that CaO occurs mostly as calcite. This is supported by a positive correlation between the

Table 4. Sulfur isotope compositions of hand-picked grains of pyrite.

Sample	$\delta^{34}S$ (‰)
M163	+2.7
M178-X[a]	+28.1
M178-Y[a]	+25.2
M181	+12.2
M197-X[a]	+18.5
M197-Y[a]	+14.2
M207	+7.2
AC1	+15.2
AC8	+18.5

[a]X and Y in samples of M178 and M197 are different grains.

Table 5. Carbon isotope compositions of organic matter.

Sample	$\delta^{13}C_{PDB}$ (‰)
AC1	–23.8
AC2	–29.2
AC3	–27.2
AC4	–28.3
AC5	–28.4
AC6	–26.5
AC7	–29.3
AC8	–25.5

Note: PDB, Pee Dee Belemnite.

Fig. 8. Bulk rock compositions on Al_2O_3 – (Na_2O + CaO*) – K_2O ternary diagram. Data sources: North American Shale Composite (NASC; Condie 1993), upper continental crust (UCC; Rudnick and Gao 2004). [Colour online.]

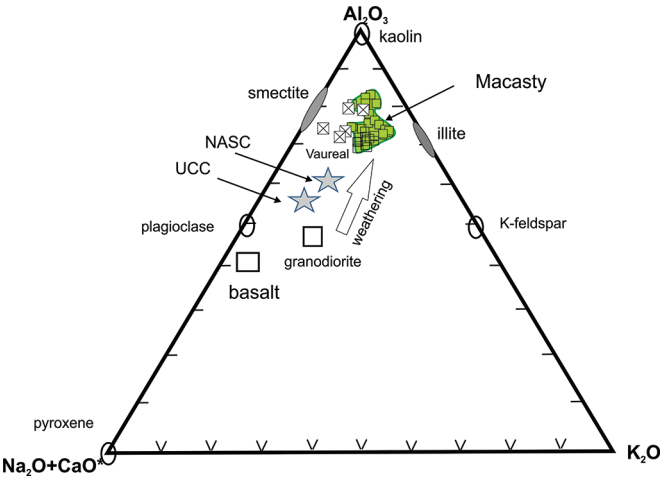

abundance of CaO and calcite calculated from the values of LOI-1050 °C. (Fig. 4).

Thin-section examination and XRD did not show any Mg-bearing minerals in the Macasty samples, but the concentrations of MgO vary from 1.36 to 3.1 wt.% on a volatile-free basis in most samples. Possible hosts of MgO are illite and calcite. Ilite may contain 3–5 wt.% MgO. Using the average composition of illite, 7.3 wt.% K_2O and 4 wt.% MgO, the amounts of MgO hosted by illite are calculated to vary from 0.12 to 1.77 wt.%. The remaining MgO is considered to be in calcite. Molecular ratios of Mg/Ca of calcite are calculated to be 0.02–0.04 in most samples. Several samples (M171, M93, M194, M190, M200) show ratios of Mg/Ca ranging from 0.08 to 0.13. The values are high for calcite, suggesting that these samples likely contain minor dolomite.

Bulk rock compositions of the Macasty shale show the molar ratios of Sr/Ca multiplied by 1000 varying from 1.3 to 12 with a median value of 4.5. The values around 1 are comparable to the ratios of 1–3 for marine carbonate (Lear et al. 2003; Gillikin et al. 2005). The values for most samples are high, suggesting that Sr is hosted by other minerals, such as mica and illite, where Sr replaces K.

Diagenesis

The chemical composition of the Macasty shale is used to evaluate the detritus sources, but the composition may change after deposition. Therefore, the effect of diagenesis on compositions of sediments is evaluated first. Thin-section examination shows that calcite forms spherical grains within samples. Cone-in-cone structured calcite is common along bedding planes, suggesting that calcite crystallized during early diagenesis (Kulkarni et al. 2013). Unlike pyrite, calcite does not crosscut bedding planes, suggesting that calcite crystallized before the lithification of the sediments.

Marine carbonate shows a large shift in $\delta^{13}C$, from around 0‰ to +6‰ at the terminal Ordovician (e.g., Ainsaar et al. 2010). The $\delta^{13}C$ values for calcite from the Macasty shale range from –2.2‰ to +0.6‰ (Table 2). They are consistent with the source from marine carbonate of the early Katian stage before the large carbon isotope excursion started in the Hirnantian stage because the values are similar to those from elsewhere (Shields et al. 2003; Ainsaar et al. 2010).

Although $\delta^{13}C$ values of calcite likely represent that of marine carbonate, $\delta^{18}O$ values of calcite are lower than the marine carbonate value. Possible causes for lower $\delta^{18}O$ values for calcite are an incursion of meteoric water, low $\delta^{18}O$ in seawater, and elevated temperatures at the time of calcite crystallization. We discount the first possibility. Calcite formed in fresh waters commonly shows low $\delta^{13}C$ values because dissolved inorganic carbon in fresh waters is low in ^{13}C compared with marine carbonate. The Macasty calcite has $\delta^{13}C$ values similar to that of marine carbonate, rejecting this possibility. The second possibility is low $\delta^{18}O$ in seawater during the Ordovician period. Qing and Veizer (1994) and Veizer and Prokoph (2015) proposed ~–4‰ relative to standard mean ocean water for seawater during the Caradoc-Ashgill epoch in the Late Ordovician time, which corresponds to the time of deposition of Macasty shale. Using the ocean water value, equilibrium isotope temperatures for calcite are calculated to range from 16 to 34 °C. Alternatively, if the seawater had an oxygen isotope composition similar to the present-day value, the equilibrium isotope temperatures are calculated to be between 42 and 54 °C, which correspond to a depth of 1.5–2 km using a geothermal gradient of continental margin, 0.025–0.03 °C/m (e.g., Beaumont 1981). Either way, the calcite crystallized at low temperatures, <60 °C, which is consistent with the lack of any high-temperature minerals.

Coarse cubes (~1 mm) of pyrite are also present along bedding planes and also narrow (<1 mm) fractures, suggesting that these coarse grains of pyrite crystallized during the late diagenesis and after the lithification of the sediments. Heterogeneous S-isotope compositions of pyrite suggest multiple generations of crystallization from solution under low water/rock ratios.

Provenance

The location and age of the Macasty shale in the Anticosti Basin suggest several possible provenances. The most proximal source is Grenvillian rocks to the north, west, and south of the Anticosti Basin (Figs. 1, 2). The Grenvillian rocks formed a large land north of the Basin during Ordovician time (Fig. 2). The Grenvillian rocks also underlie the Anticosti Basin at present. The second source is Taconian igneous rocks. The area to the east of the Anticosti Basin has had a complex geological history since Early Cambrian time, including the opening of the Iapetus Ocean, obduction and accretion of an island arc, and the formation of a continental arc. Abundant igneous rocks, including ophiolitic rocks, thrust slices of oceanic rocks, subduction-related mafic-intermediate rocks, and granites, were introduced to the eastern margin of North America during the Taconian orogenic event (e.g., Hiscott 1978; Dunning et al. 1991; Huff et al. 1992; Whalen et al. 1996). Voluminous mafic magmatism during the orogenic event likely contributed to a decline in $^{87}Sr/^{86}Sr$ for marine Sr during the Ordovician period (e.g., Young et al. 2009). Furthermore, violent explosive felsic volcanism is recorded as ash beds in many places in Appalachia, including Georgia, Alabama, Kentucky, Tennessee, and Pennsylvania (e.g., Samson et al. 1989).

The third possible source of detritus is allochthonous slices that were thrust inland during the Taconic orogeny. A series of ophiolitic massifs, crosscutting granites, and associated metamorphic rocks occurred along the Baie Verte – Brompton line, the Taconian suture between Laurentia and the early Paleozoic peri-Laurentian oceanic terranes. These ophiolitic massifs are represented by the Lac-Brompton ophiolite and the Rivière-des-Plante Ultramafic Complex in southern Quebec, and the Nadeau Ophiolitic Mélange in the Gaspé Peninsula (De Souza et al. 2012). Other massifs are present in eastern New York and western Massachusetts (Ratcliffe 1987). If allochthons supplied the detritus for the Macasty sediments, such dynamic tectonic activity likely fostered physical erosion to produce coarse-grained detritus for texturally immature sediments. This is not consistent with the fine-grained organic-rich sediments in the Macasty basin. Therefore, we do not consider the allochthons to be the potential source of the Macasty shale.

Neodymium isotope compositions are very useful in evaluating the provenances of siliclastic sedimentary rocks because sediment transport processes are not expected to result in isotopic fractionation. Therefore, Nd isotope compositions of sedimentary rocks of many different ages have been used widely to evaluate the provenance rocks of sedimentary rocks (e.g., Patchett and Ruiz 1989; Andersen and Samson 1995; Dickin 2000; Clift et al. 2002). In this study, $^{143}Nd/^{144}Nd$ values for the Macasty sediments and possible provenance rocks that supplied detritus are calculated at 450 Ma (Fig. 9). The Grenville Province is divided into several terranes. In general, the northern part of the province contains old rocks, especially rocks close to the Archean Superior Province (Ashwal et al. 1986; Martin and Dickin 2005). Grenville rocks north of the St. Lawrence River belong to the Labradoria and Quebecia terranes, which are highly metamorphosed, subduction-related, igneous rocks formed at ~1.7 to 1.5 Ga (Dickin 2000; van Breemen and Corriveau 2005). Grenvillian rocks due north and closest to Anticosti Island belong to the Labradoria terrane (McLelland et al. 2010). The Nd isotope compositions of these rocks at 450 Ma are very similar to those of the Macasty shale (Fig. 9). The southeast Labrador area, farther north of the Labradoria and Quebecia terranes, contains older rocks, shown as low $\varepsilon Nd(t)$ (Fig. 9). Grenvillian rocks are also exposed south of the St. Lawrence River. They include the rocks in the Adirondack Lowlands and Highlands (Westeneys et al. 1999) and the Blair River Complex on Cape Breton Island (Barr and Hegner 1992). The Adirondack Lowlands are considered to be an extension of the Labradoria terrane north of the St. Lawrence River (Westeneys et al. 1999) and to be slightly older than the Adirondack Highlands, which have higher $\varepsilon Nd(t)$ (Daly and McLelland 1991) (Fig. 9).

Grenvillian rocks on Cape Breton Island show significantly higher $^{143}Nd/^{144}Nd(t)$ values than the values for the Macasty shale (Fig. 9). Early Ordovician felsic igneous rocks in the Aspy and Bras d'Or terranes, south of the Blair River Complex on Cape Breton Island, have a juvenile geochemical signature showing chondritic Nd isotope compositions (Barr and Hegner 1992). The Dunnage zone and Humber zone east and south of the Anticosti Basin extend from Cape Breton Island to Newfoundland, and the zones are considered to have formed at around 471 Ma (MacLachlan and Dunning 1998). The igneous rocks in the Dunnage and Humber

Fig. 9. Box-whisker plots of $^{143}Nd/^{144}Nd$ and $\varepsilon Nd(t)$ of the Macasty shale (red), possible provenance rocks (pink), and contemporaneous Ordovician sedimentary rocks (green). The values of εNd (450 Ma) and $^{143}Nd/^{144}Nd$ at 450 Ma are calculated from the present-day $^{143}Nd/^{144}Nd$ and $^{147}Sm/^{144}Nd$ tabulated in the references. Data sources: Gneisses of the Labradorian and Quebecia terranes (Dickin 2000), Late Proterozoic to early Paleozoic rocks in Cape Breton Island (Barr and Hegner 1992), ranitoids in the Humber-Dunnage zone in the Gaspé Peninsula and New Brunswick (Whalen et al. 1997), Adirondack Highlands (Daly and McLelland 1991), widespread K-bentonite layers of 457 Ma (Samson et al. 1989), Utica shale in New York (Andersen and Samson 1995), other Ordovician sedimentary rocks in New York, Virginia, and Tennessee (Andersen and Samson 1995), and the Austin Glenn Member of the Normanskill Formation (Bock et al. 1998). Small values depicted below quartile boxes are the numbers of analyses. Note that the Labradorian rocks in the Kegaska area are exposed directly north of Anticosti Island, and they are the closest in distance to the Macasty Basin. [Colour online.]

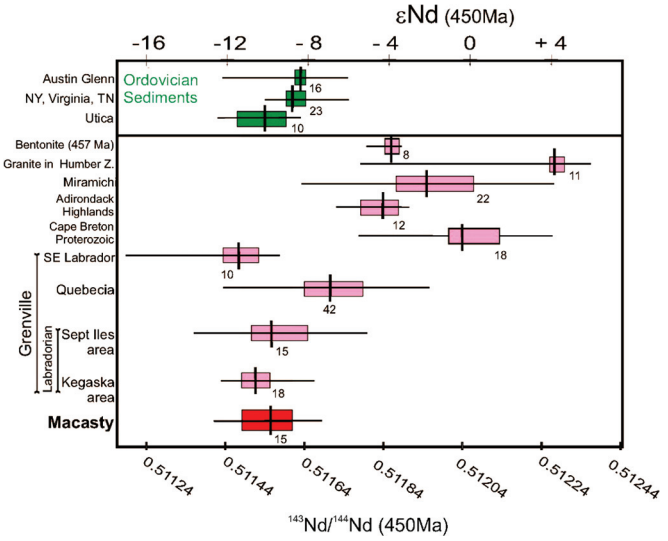

zones show relatively high $^{143}Nd/^{144}Nd(t)$ (Barr and Hegner 1992). Although these igneous rocks assimilated Grenvillian basement rocks during their ascent, the overall geochemical signatures of these rocks are juvenile, with high $^{143}Nd/^{144}Nd$, and the values of $\varepsilon Nd(t)$ are higher than those for the Macasty shale. Therefore, Paleozoic igneous rocks contemporaneous with the Macasty shale do not appear to be a significant contributor to the basin. The comparison of Nd isotope compositions suggests that the predominant provenance of the Macasty shale is the Labradorian rocks, which are widely exposed north, northeast, and northwest of Anticosti Island.

Weathering of source rocks in the provenance

The occurrence of kaolinite as a detrital mineral suggests that the rocks in the provenance underwent intense weathering. This is consistent with the generally warm, wet climate that prevailed during the Ordovician period (Thompson and Kah 2012).

The weathering conditions of the source rocks in the provenance were evaluated quantitatively using the ternary diagram of $Al_2O_3 - (Na_2O + CaO^*) - K_2O$ (Fig. 8). The rocks plot close to the Al apex, suggesting that the source rocks underwent high degrees of chemical weathering. Although Na contents are high in felsic gneissic rocks, its low concentrations in the Macasty rocks reflect intense weathering. The detrital minerals were not affected by high Na in depositioned and diagenesis in marine environments. Therefore, their plot close to the Al apex reflects the composition of detrital material caused by intense weathering in the provenance rocks.

The stratigraphic variation of the intensity of weathering is evaluated using the chemical index of alteration (CIA) (Fig. 4). The value of CIA is a molecular proportion of $[Al_2O_3/(Al_2O_3 + CaO^* + Na_2O + K_2O)] \times 100$, where CaO^* represents CaO in silicate minerals. The index gives a degree of weathering at the provenance (e.g., Nesbitt and Young 1982; Price and Velbel 2003; Shao et al. 2012). The NASC by Condie (1993) has a much lower CIA value than does the Macasty shale (Fig. 4), suggesting that the source rocks for the Macasty shale experienced high degrees of chemical weathering. This is consistent with the occurrence of kaolinite in the XRD pattern of the samples. If the source rocks had intense weathering before the deposition of the Macasty shale, but moderate weathering during the deposition, the values of CIA should be lower in the upper stratigraphic section of the Macasty shale. The values of CIA change slightly but remain high, above 70 (Fig. 4), suggesting that the source rocks experienced intense weathering before erosion of the detritus to be transported to the Anticosti Basin.

The Grenville rocks were exposed for a long geological time after their formation in the mid-Proterozoic time. A long time of exposure and erosion of rocks in the Grenville terrane likely produced a low, gentle relief during the deposition of the Macasty shale in the Late Ordovician time. This long period of exposure likely allowed Grenvillian rocks to undergo intense chemical weathering before being physically eroded from the site.

Depositional environments

Geochemical parameters, including a high abundance of organic matter and pyrite, all suggest that the depositional site was anoxic. This is well illustrated by Th/U ratios (Fig. 4). Uranium changes its valence from highly soluble U^{+6} in oxidizing water to insoluble U^{+4} under anoxic conditions. On the other hand, Th is not soluble in low-temperature aqueous solutions, and it is transported from the source rocks in terrigenous fragments to depositional sites. Igneous rocks and terrigenous material have ratios of Th/U of between 3.5 and 4 (Taylor and McLennan 1985). The Macasty shale shows very low Th/U ratios, lower than 0.8 (Fig. 4). The low ratios are a result of high U, which was transported as U^{6+} and was reduced and fixed in the sediments under anoxic conditions.

The reduced condition is further supported by a positive correlation between K and V (Fig. 3B). Vanadium is +3 under reduced conditions, allowing it to be incorporated into mica.

The total organic carbon contents show a broad positive correlation with the total sulfur contents (Fig. 7). The values are close to those observed in normal marine sediments, supporting the linkage of fixation of sulfide sulfur and accumulation of organic carbon (e.g., Raiswell and Berner 1985; Jenkyns 1988). The concentrations of Fe and S show a broad positive correlation, and the values are similar to those of many euxinic sediments, shown as a dashed line in Fig. 7, as observed by Jenkyns (1988).

The sulfide phase is pyrite in hand specimens and also in thin sections. Higher Fe contents compared with sulfur (Fig. 7) are explained by Fe hosted by other phases. For example, illite contains 2.05 wt.% Fe_2O_3 as total Fe. Using the K_2O contents of the rocks, Fe in illite is calculated to be 0.22–0.91 wt.% Fe_2O_3.

Fine (<0.01 mm) grains of pyrite are disseminated in the samples. Some form framboidal pyrite. The texture and distribution of pyrite suggest that sulfide sulfur was introduced during the deposition or early diagenesis of the Macasty shale. Sulfur isotope compositions of fine dissemination of pyrite show ~–2.4‰, with no significant change in the stratigraphic positions of samples. The data support a similar environment during deposition of the Macasty shale.

Marine sulfate shows a large variation, from +15‰ to +30‰, in the Early-Mid Ordovician and also at the end of Ordovician (e.g., Thompson and Kah 2012; Jones and Fike 2013). The precise $\delta^{34}S$ value of marine sulfate during deposition of the Macasty shale is not certain, but it is most likely around +20‰ to +25‰ (Claypool et al. 1980; Jones and Fike 2013). This indicates an apparent isotope

fractionation between sulfide sulfur and sulfate of about 20‰ to 30‰. The isotope fractionation is small compared with that typically observed in marine sediments during anoxic and euxinic conditions (e.g., Neretin et al. 2003; Sorensen and Canfield 2004). This small difference may be attributed to a low sulfate concentration in the pore water of organic-rich sediments because of rapid consumption of marine sulfate, although abundant planktonic marine fossils in the Macasty shale suggest a physical connection between the sedimentary basin and the ocean. We suggest that slow diffusion of sulfate through fine-grained organic-rich sediments and fast reduction kept the concentrations of dissolved sulfate low in pore water. Similar sulfur isotope compositions of disseminated pyrite suggest that the conditions remained similar throughout the deposition of the Macasty shale.

High levels of bioproductivity were likely promoted under warm conditions in the basin, as supported by intense weathering of the source rocks, described earlier in the text. It is also consistent with the warm climate that prevailed during the Ordovician period (e.g., Munnecke et al. 2010). Furthermore, carbonatites are abundant on the north shore of the St. Lawrence River. Many were emplaced at around 600 Ma (e.g., Doig and Barton 1968) and were likely exposed during the deposition of Macasty shale. Carbonatites contain abundant apatite and may have supplied phosphates, an important nutrient for organic productivity, to the basin. Finely laminated, undisturbed bedding with the superb preservation of graptolites in the Macasty shale also supports the interpretation of prolonged anoxic conditions.

Comparison with other Ordovician sedimentary rocks in the region

The $\varepsilon Nd(t)$ values for the Macasty shale are similar to those of other Ordovician sedimentary rocks (Fig. 9). The values for the Macasty shale range from –12.3 at the base to –9.5 at the top near the Vauréal Formation (Table 3). Very similar values are reported for the Utica shale in northern New York by Andersen and Samson (1995), from –12.6 to –11.0 in Lower Utica shale and from –9.7 to –8.5 in Upper Utica shale. Andersen and Samson (1995) interpreted that this slight increase in $\varepsilon Nd(t)$ in younger units reflects a contribution of juvenile sources, such as exotic terranes. Although there is no evidence rejecting or supporting the existence of allochthons with a juvenile source, there are other possibilities to explain this slight change. Within the Grenville Province, rocks in the southern terranes are younger, with higher $\varepsilon Nd(t)$ values. For example, the Adirondack Highlands have higher $\varepsilon Nd(t)$ than does the Labradorian terrane on the north shore of the St. Lawrence River (Fig. 9). Mafic rocks have higher Sm/Nd than do felsic rocks, and $^{143}Nd/^{144}Nd$ for mafic rocks have higher $\varepsilon Nd(t)$ than do contemporaneous felsic rocks. Deeper crustal rocks are usually more mafic than shallower crustal rocks. Gradual unroofing of deeper rocks in the provenance during the development of the sedimentary basins may also explain increasing $\varepsilon Nd(t)$ values for upper parts of the sedimentary rocks.

Andersen and Samson (1995) reported Nd isotope compositions of Ordovician sedimentary rocks from southern New York, Virginia, and Tennessee. The values of $\varepsilon Nd(t)$ are slightly higher than those for the Macasty and Utica shales (Fig. 9) and are similar to the values for the Austin Glen Member of the Normanskill Formation in eastern New York as reported by Bock et al. (1998). Overall low $\varepsilon Nd(t)$ for the Ordovician shale confirms that Grenvillian rocks are the main contributor of the terrigenous material, but that the slightly higher $\varepsilon Nd(t)$ values for sedimentary rocks farther south in the United States are attributable to younger ages of Grenvillian rocks in the southern United States and a possible minor contribution of Taconian rocks. The Grenvillian rocks in southern Quebec (Labradorian and Quebecia terranes) formed at 1.7–1.5 Ga, and those in central Virginia and Texas at around 1.1 Ga (Patchett and Ruiz 1989). This explains why Grenvillian rocks in the United States have higher $\varepsilon Nd(t)$ values at 450 Ma. It is also possible that Ordovician basins received minor contributions of Taconian rocks. The Macasty and Utica basins were surrounded by Grenvillian rocks, whereas rocks in the southern United States are on the eastern margin of the North American continent and are likely exposed to Taconian igneous rocks.

The widespread occurrence of Upper Ordovician ash beds in eastern Laurentia (Huff 2008) suggests that explosive arc volcanism was probably contemporaneous with the accumulation of the Macasty shale in the Anticosti Basin. The geochemistry of the Macasty shale, however, does not show evidence for such orogenic activity in the Anticosti Basin during early to mid-Katian. The lack of evidence for Taconic orogenic activity suggests that topographic features likely impeded the transport of material from the active orogens to the basin.

Conclusions

The provenance that supplied detritus for the Macasty shale is predominantly granitic–gneiss terrane of the Grenville Province and most likely the Labradoria terrane. The Grenvillian rocks were exposed on a land mass just north of the Anticosti Basin during the deposition. These rocks were intensely weathered to form kaolinite before being erosioned to the basin. The deposition of the Macasty shale is considered to be synchronous with the Taconic orogeny, which brought allochthonous slices to the east to the Anticosti Basin and produced voluminous igneous rocks and also explosive volcanic rocks. These rocks, related to the Taconic orogeny, which include explosive volcanic rocks, did not make a significant contribution to the detritus of the Macasty shale.

The water in the Anticosti Basin during the deposition of the Macasty shale was likely stratified where fertile bioproductivity in oxygenated shallow water was underlain by anoxic water. This allowed the preservation of abundant organic matter and relatively high $\delta^{34}S$ values for pyrite in sediments throughout the succession. The deposition of the Macasty shale is followed by diagenesis at low temperatures, <60 °C, where the sediments were cemented by calcite and silica leached from radiolarian fossils.

Acknowledgements

This project was supported by Discovery Grants from the Natural Science Engineering Research Council of Canada to K.H. and A.D. We thank George Mrazek for section making, Atul Kulkarni for sample processing, Glenn Poirier for his assistance during the SEM analysis, Tara Kell for XRF and XRD analysis, Paul Middlestead for stable isotope analysis of samples, and Elizabeth-Anne Spencer for her help with Nd–Sm chemistry and thermal ionization mass spectrometry. The bulk of the geochemical data presented in this manuscript were obtained by Janice Pedro during her B.Sc. thesis project.

References

Ainsaar, L., Kaljo, D., Martma, T., Meidla, T., Männik, P., Nõlvak, J., and Tinn, O. 2010. Middle and Upper Ordovician carbon isotope chemostratigraphy in Baltoscandia: a correlation standard and clues to environmental history. Palaeogeography, Palaeoclimatology, Palaeoecology, **294**: 189–201. doi:10.1016/j.palaeo.2010.01.003.

Andersen, C.B., and Samson, S.D. 1995. Temporal changes in Nd isotope compositions in sedimentary rocks in the Sevier and Taconic foreland basins: increasing influence of juvenile sources. Geology, **23**: 983–986. doi:10.1130/0091-7613(1995)023<0983:TCINIC>2.3.CO;2.

Ashwal, L.D., Wooden, J.L., and Emslie, R.F. 1986. Sr, Nd, and Pb isotopes in Proterozoic intrusives astride the Grenville Front in Labrador: Implications for crustal contamination and basement mapping. Geochimica et Cosmochimica Acta, **50**: 2571–2585. doi:10.1016/0016-7037(86)90211-5.

Barr, S.M., and Hegner, E. 1992. Nd isotopic compositions of felsic igneous rocks in Cape Breton Island, Nova Scotia. Canadian Journal of Earth Sciences, **29**(4): 650–657. doi:10.1139/e92-056.

Beaumont, C. 1981. Foreland basins. Geophysical Journal International, **65**: 291–329. doi:10.1111/j.1365-246X.1981.tb02715.x.

Berner, R.A., and Raiswell, R. 1983. Burial of organic carbon and pyrite sulfur in

sediments over Phanerozoic time: A new theory. Geochimica et Cosmochimica Acta, **47**(5): 855–862. doi:10.1016/0016-7037(83)90151-5.

Bock, B., McLennan, S.M., and Hanson, G.N. 1998. Geochemistry and provenance of the Middle Ordovician Austin Glen Member (Normanskill Formation) and the Taconian Orogeny in New England. Sedimentology, **45**: 635–655. doi:10.1046/j.1365-3091.1998.00168.x.

Castonguay, S., Ruffet, G., and Tremblay, A. 2007. Dating polyphaser deformation across low-grade metamorphic belts: an example based on $^{40}Ar/^{39}Ar$ muscovite age constraints from the southern Quebec Appalachians, Canada. Geological Society of America Bulletin, **119**: 978–992. doi:10.1130/B26046.1.

Chen, Z., Lavoie, D., Jiang, C., Duchesne, M.J., and Malo, M. 2016. Geological characteristics and petroleum resource assessment of the Macasty Formation, Anticosti Island, Québec, Canada. Geological Survey of Canada Open File 8018, 67 pp.

Chukhrov, F.V., Ermilova, L.P., Churikov, V.S., and Nosik, L.P. 1980. The isotopic composition of plant sulfur. Organic Geochemistry, **2**: 69–75. doi:10.1016/0146-6380(80)90022-4.

Claypool, G.E., Holser, W.T., Kaplan, I.R., Sakai, H., and Zak, I. 1980. The age curves of sulfur and oxygen isotopes in marine sulfate and their mutual interpretation. Chemical Geology, **28**: 199–260. doi:10.1016/0009-2541(80)90047-9.

Clift, P.D., Lee, J.I., Hildebrand, P., Shimizu, N., Layne, G.D., Blusztajn, J., et al. 2002. Nd and Pb isotope variability in the Indus River System: implications for sediment provenance and crustal heterogeneity in the Western Himalaya. Earth and Planetary Science Letters, **200**: 91–106. doi:10.1016/S0012-821X(02)00620-9.

Comeau, F.-A., Kirkwood, D., Malo, M., Asselin, E., and Bertrand, R. 2004. Taconian mélanges in the parautochthonous zone of the Quebec Appalachians revisted: implications for foreland basin and thrust belt evolution. Canadian Journal of Earth Sciences, **41**(12): 1473–1490. doi:10.1139/e04-083.

Condie, K.C. 1993. Chemical composition and evolution of the upper continental crust: Contrasting results from surface samples and shales. Chemical Geology, **104**: 1–37. doi:10.1016/0009-2541(93)90140-E.

Daly, J.S., and McLelland, J.M. 1991. Juvenile Middle Proterozoic crust in the Adirondack Highlands, Grenville province, northeastern North America. Geology, **19**: 119–122. doi:10.1130/0091-7613(1991)019<0119:JMPCIT>2.3.CO;2.

De Souza, S., Tremblay, A., Ruffet, G., and Pinet, N. 2012. Ophiolite obduction in the Quebec Appalachians, Canada — $^{40}Ar/^{39}Ar$ age constraints and evidence for syn-tectonic erosion and sedimentation. Canadian Journal of Earth Sciences, **49**(1): 91–110. doi:10.1139/e11-037.

Dhuime, B., Hawkesworth, C., and Cawood, P. 2011. When continents formed. Science, **331**: 154–155. doi:10.1126/science.1201245.

Dickin, A.P. 2000. Crustal formation in the Grenville Province: Nd-isotope evidence. Canadian Journal of Earth Sciences, **37**(2–3): 165–181. doi:10.1139/e99-039.

Dietrich, J., Lavoie, D., Hannigan, P., Pinet, N., Castonguay, P., Giles, P., and Hamblin, A.P. 2011. Geological setting and resource potential of conventional petroleum plays in Paleozoic basins in eastern Canada. Bulletin Canadian Petroleum Geology, **59**: 54–84. doi:10.2113/gscpgbull.59.1.54.

Doig, R., and Barton, J.M., Jr. 1968. Ages of carbonatites and other alkaline rocks in Québec. Canadian Journal of Earth Sciences, **5**(6): 1401–1407. doi:10.1139/e68-139.

Dunning, G.R., Swinden, H.S., Kean, B.F., Evans, D.T.W., and Jenner, G.A. 1991. A Cambrian island arc in Iapetus: geochronology and geochemistry of the Lake Ambrose volcanic belt, Newfoundland Appalachians. Geological Magazine, **128**: 1–17. doi:10.1017/S0016756800018008.

Gillikin, D.P., Lorrain, A., Navez, J., Taylor, J.W., Andre, L., Keppens, E., et al. 2005. Strong biological controls on Sr/Ca ratios in aragonitic marine bivalve shells. Geochemistry, Geophysics, Geosystems, **6**(5). doi:10.1029/2004GC000874.

Haskin, M.A., and Haskin, L.A. 1966. Rare earths in European shales: a redetermination. Science, **154**: 507–509. doi:10.1126/science.154.3748.507.

Heiri, O., Lotter, A.F., and Lemcke, G. 2001. Loss on ignition as a method for estimating organic and carbonate content in sediments: reproducibility and comparability of results. Journal of Paleolimnology, **25**: 101–110. doi:10.1023/A:1008119611481.

Hiscott, R.N. 1978. Provenance of Ordovician deep-water sandstones, Tourelle Formation, Quebec, and implications for initiation of the Taconic orogeny. Canadian Journal of Earth Sciences, **15**(10): 1579–1597. doi:10.1139/e78-163.

Huff, W.D. 2008. Ordovician K-bentonites: Issues in interpreting and correlating ancient tephras. Quaternary International, **178**: 276–287. doi:10.1016/j.quaint.2007.04.007.

Huff, W.D., Bergstrom, S.M., and Kolata, D.R. 1992. Gigantic Ordovician volcanic ash fall in North America and Europe: Biological, tectonomagmatic and event-stratigraphic significance. Geology, **20**: 875–878. doi:10.1130/0091-7613(1992)020<0875:GOVAFI>2.3.CO;2.

Jenkyns, H.C. 1988. The early Toarcian (Jurassic) anoxic event: stratigraphic sedimentary, and geochemical evidence. American Journal of Science, **288**: 101–151. doi:10.2475/ajs.288.2.101.

Jones, D.S., and Fike, D.A. 2013. Dynamic sulfur and carbon cycling through the end-Ordovician extinction revealed by paired sulfate-pyrite $\delta^{34}S$. Earth and Planetary Science Letters, **363**: 144–155. doi:10.1016/j.epsl.2012.12.015.

Kulkarni, A.R., Hattori, K., and Desrochers, A. 2013. Depositional Environments of Organic-Rich Calcareous Shale in the Western Anticosti Basin: the Upper Ordovician Macasty Formation, Quebec, Canada. *In* Proceedings of the AAPG Annual Convention and Exhibition, Pittsburgh, Pennsylvania, May 19–22, 2013. Search and Discovery Article No. 10571.

Lavoie, D. 2008. Appalachian foreland basin in Canada. *In* Sedimentary Basins of the United States and Canada. Vol. 5, 1st ed. *Edited by* A.D. Miall. pp. 65–103.

Lavoie, D., Pinet, N., Dietrich, J., Hannigan, P., Castonguay, S., Hamblin, A.P., and Giles, P. 2009. Petroleum resource assessment, Paleozoic successions of the St. Lawrence Platform and Appalachians of eastern Canada. Geological Survey of Canada Open File 6174, 273 pp.

Lavoie, D., Pinet, N., Bordeleau, G., Ardakani, O.H., Ladevèze, P., Duchesne, M.J., et al. 2016. The Upper Ordovician black shales of southern Quebec (Canada) and their significance for naturally occurring hydrocarbons in shallow groundwater. International Journal of Coal Geology, **158**: 44–64. doi:10.1016/j.coal.2016.02.008.

Lear, C.H., Elderfield, H., and Wilson, P.A. 2003. A Cenozoic seawater Sr/Ca record from benthic foraminiferal calcite and its application in determining global weathering fluxes. Earth and Planetary Science Letters, **208**: 69–84. doi:10.1016/S0012-821X(02)01156-1.

Long, D.G.F. 2007. Tempestite frequency curves: a key to Late Ordovician and Early Silurian subsidence, sea-level change, and orbital forcing in the Anticosti foreland basin, Québec, Canada. Canadian Journal of Earth Sciences, **44**(3): 413–431. doi:10.1139/e06-099.

Lyons, T.W. 1997. Sulfur isotopic trends and pathways of iron sulfide formation in upper Holocene sediments of the anoxic Black Sea. Geochimica et Cosmochimica Acta, **61**: 3367–3382. doi:10.1016/S0016-7037(97)00174-9.

Lyons, T.W., and Berner, R.A. 1992. Carbon-sulfur-iron systematics of the uppermost deep-water sediments of the Black Sea. Chemical Geology, **99**: 1–27. doi:10.1016/0009-2541(92)90028-4.

MacLachlan, K., and Dunning, G. 1998. U–Pb ages and tectono-magmatic evolution of Middle Ordovician volcanic rocks of the Wild Bight Group, Newfoundland Appalachians. Canadian Journal of Earth Sciences, **35**(9): 998–1017. doi:10.1139/e98-050.

Malo, M. 2004. Paleogeography of the Matapédia basin in the Gaspé Appalachians: initiation of the Gaspé Belt successor basin. Canadian Journal of Earth Sciences, **41**(5): 533–570. doi:10.1139/e03-100.

Martin, C., and Dickin, A.P. 2005. Styles of Proterozoic crustal growth on the southeast margin of Laurentia: Evidence from the central Grenville Province northwest of Lac St. Jean, Québec. Canadian Journal of Earth Sciences, **42**(10): 1643–1652. doi:10.1139/e05-052.

McLaughlin, P.I., and Brett, C.E. 2007. Signatures of sea-level rise on the carbonate margin of a late Ordovician foreland basin: A case study from the Cincinnati arch, USA. Palaios, **22**(3): 245–267. doi:10.2110/palo.2006.p06-106.

McLaughlin, P., Emsbo, P., Desrochers, A., Bancroft, A.M., Brett, C., Premo, W., et al. 2016. Refining two kilometers of Ordovician chronostratigraphy beneath Anticosti Island utilizing integrated chemostratigraphy. Canadian Journal of Earth Sciences, **53**(8): 865–874. doi:10.1139/cjes-2015-0242.

McLelland, J.M., Selleck, B.W., and Bickford, M.E. 2010. Review of the Proterozoic evolution of the Grenville Province, its Adirondack outlier, and the Mesoproterozoic inliers of the Appalachians. *In* From Rodinia to Rangea: The Lithotectonic Record of the Appalachian Region. *Edited by* R.P. Tollo, M.J. Bartholomew, J.P. Hibbard, and P.M. Karabinos. Geological Society of America Memoir 206, pp. 1–29.

Munnecke, A., Calner, M., Harper, D.A.T., and Servais, T. 2010. Ordovician and Silurian sea-water chemistry, sea level, and climate: a synopsis. Palaeogeography, Palaeoclimatology, Palaeoeclogy, **296**: 389–413. doi:10.1016/j.palaeo.2010.08.001.

Neretin, L.N., Böttcher, M.E., and Grinenko, V.A. 2003. Sulfur isotope geochemistry of the Black Sea water column. Chemical Geology, **200**: 59–69. doi:10.1016/S0009-2541(03)00129-3.

Nesbitt, W., and Young, G.M. 1982. Early Proterozoic climates and plate motions inferred from major element chemistry of lutites. Nature, **299**: 715–717. doi:10.1038/299715a0.

Ogrinc, N., Gontolan, G., Faganeli, J., and Covelli, S. 2005. Carbon and nitrogen isotope compositions of organic matter in coastal marine sediments (the Gulf of Trieste, N. Adriatic Sea): indicators of sources and preservation. Marine Chemistry, **95**: 163–181. doi:10.1016/j.marchem.2004.09.003.

Patchett, J., and Ruiz, J. 1989. Nd isotopes and the origin of Grenville-age rocks in Texas: Implications for Proterozoic evolution of the United States midcontinent region. Journal of Geology, **97**: 685–695. doi:10.1086/629352.

Pinet, N., Keating, P., Lavoie, D., Dietrich, J., Duchesne, M.J., and Brake, V. 2012. Revising the Appalachian structural front and offshore Anticosti Basin (Northern Gulf of St. Lawrence, Canada) by integrating old and new geophysical datasets. Marine and Petroleum Geology, **32**: 50–62. doi:10.1016/j.marpetgeo.2011.12.004.

Price, J.R., and Velbel, M.A. 2003. Chemical weathering indices applied to weathering profiles developed on heterogeneous felsic metamorphic parent rocks. Chemical Geology, **202**: 397–416. doi:10.1016/j.chemgeo.2002.11.001.

Qing, H., and Veizer, J. 1994. Oxygen and carbon isotopic composition of Ordovician brachiopods: Implications for coeval seawater. Geochimica et Cosmochimica Acta, **58**(20): 4429–4442. doi:10.1016/0016-7037(94)90345-X.

Raiswell, R., and Berner, R.A. 1985. Pyrite formation in euxinic and semi-euxinic sediments. American Journal of Science, **285**: 710–724. doi:10.2475/ajs.285.8.710.

Ratcliffe, N.M. 1987. Basaltic rocks in the Rensselaer Plateau and Chatham slices of the Taconic allochthon: Chemistry and tectonic setting. Geological Society America Bulletin, **99**: 511–528. doi:10.1130/0016-7606(1987)99<511:BRITRP>2.0.CO;2.

Riva, J. 1969. Middle and Upper Ordovician graptolite faunas of the St. Lawrence Lowelands and of Anticosti Island. *In* North North Atlantic Geology and Continental Drift. *Edited by* K. Kay. American Association of Petroleum Geologists Memoir 12, pp. 513–556.

Rudnick, R.L., and Gao, S. 2004. Composition of the continental crust. *In* Treatise on Geochemistry. 2nd ed. *Edited by* K.K. Turekian and H.D. Holland. Elsevier, Vol. 3, pp. 1–64.

Samson, S.D., Patchett, P.J., Roddick, J.C., and Parrish, R.R. 1989. Origin and tectonic setting of Ordovician bentonites in North America: Isotopic and age constraints. Geological Society of America Bulletin, **101**: 1175–1181. doi:10.1130/0016-7606(1989)101<1175:OATSOO>2.3.CO;2.

Schuchert, C., and Twenfofel, W.H. 1910. Ordovicic-Siluric section of the Mingan and Anticosti Islands, Gulf of St. Lawrence. Geological Society of America Bulletin, **21**: 677–716. doi:10.1130/GSAB-21-667.

Shao, J., Yang, S., and Li, C. 2012. Chemical indices (CIA and WIP) as proxies for integrated chemical weathering in China: Inferences from analysis of fluvial sediments. Sedimentary Geology, **265–266**: 110–120. doi:10.1016/j.sedgeo.2012.03.020.

Shields, G.A., Carden, G.A., Veizer, J., Meidla, T., Rong, J., and Li, R. 2003. Sr, C, and O isotope geochemistry of Ordovician brachiopods: A major isotopic event around the Middle-Late Ordovician transition. Geochimica et Cosmochimica Acta, **67**: 2005–2025. doi:10.1016/S0016-7037(02)01116-X.

Smith, L.B., and Leone, J. 2010. Integrated Characterization of Utica and Marcellus Black Shale Gas Plays, New York State. AAPG Annual Convention and Exhibition. Search and Discovery Article No. 50289.

Sorensen, K.B., and Canfield, D.E. 2004. Annual fluctuations in sulfur isotope fractionation in the water column of a euxinic marine basin. Geochimica et Cosmochimica Acta, **68**: 503–515. doi:10.1016/S0016-7037(03)00387-9.

Taylor, S.R., and McLennan, S.M. 1985. The continental crust: its composition and evolution. Blackwell Scientific Publications, Oxford, UK, 328 pp.

Thompson, C.K., and Kah, L.C. 2012. Sulfur isotope evidence for widespread euxinia and a fluctuating oxycline in Early to Middle Ordovician greenhouse oceans. Palaeogeography, Palaeoclimatology, Palaeoecology, **131–314**: 189–214. doi:10.1016/j.palaeo.2011.10.020.

van Breemen, O., and Corriveau, L. 2005. U–Pb age constraints on arenaceous and volcanic rocks of the Wakeham Group, eastern Grenville Province. Canadian Journal of Earth Sciences, **42**(10): 1677–1697. doi:10.1139/e05-079.

van Staal, C.R. 2005. North America; Northern Appalachians. *In* Encyclopedia of Geology. *Edited by* R.C. Selley, R.M. Cocks, and I.R. Plimer. Elsevier, Oxford, UK, pp. 81–92.

Veizer, J., and Prokoph, A. 2015. Temperatures and oxygen isotopic composition of Phanerozoic oceans. Earth Science Reviews, **146**: 92–104. doi:10.1016/j.earscirev.2015.03.008.

Westeneys, H., McLelland, J., and Lumbers, S. 1999. Precise zircon geochronology in the Adirondack Lowlands and implications for revising plate-tectonic models of the Central Metasedimentary Belt and Adirondack Mountains, Grenville Province, Ontario and New York. Canadian Journal of Earth Science, **36**(6): 967–984. doi:10.1139/e99-020.

Whalen, J.B., Jenner, G.A., Longstaffe, F.J., Robert, F., and Gariepy, C. 1996. Geochemical and isotopic (O, Nd, Pb and Sr) constraints on A-type granite petrogenesis based on the Topsails igneous suite, Newfoundland Appalachians. Journal of Petrology, **37**: 1463–1489. doi:10.1093/petrology/37.6.1463.

Whalen, J.B., Rogers, N., vanSataal, C.R., Longstaffe, F.J., Jenner, G.A., and Winchester, J.A. 1997. Geochemical and isotopic (Nd, O) data from Ordovician felsic plutonic and volcanic rocks of the Miramichi Highlands: petrogenetic and metallogenic implications for the Bathurst Mining Camp. Canadian Journal of Earth Sciences, **35**(3): 237–252. doi:10.1139/e97-102.

Workman, R.K., and Hart, S.R. 2005. Major and trace element composition of the depleted MORB Mantle (DMM). Earth and Planetary Science Letters, **231**: 53–72. doi:10.1016/j.epsl.2004.12.005.

Young, S.A., Saltzman, M.R., Foland, K.A., Linder, J.S., and Kump, L.R. 2009. A major drop in seawater $^{87}Sr/^{86}Sr$ during the Middle Ordovician (Darriwilian): Links to volcanism and climate? Geology, **37**: 951–954. doi:10.1130/G30152A.1.